Published in final edited form as:
Biomaterials. 2009 September ; 30(27): 4665–4675. doi:10.1016/j.biomaterials.2009.05.033.

The use of three-dimensional nanostructures to instruct cells to produce extracellular matrix for regenerative medicine strategies

Katja Schenke-Layland[1,*], **Fady Rofail**[2], **Sanaz Heydarkhan**[3], **Jessica M. Gluck**[2], **Nilesh P. Ingle**[4], **Ekaterini Angelis**[1], **Chang-Hwan Choi**[5], **W Robb MacLellan**[1], **Ramin E Beygui**[2,6], **Richard J Shemin**[2], and **Sepideh Heydarkhan-Hagvall**[2]

[1]Cardiovascular Research Laboratories, Department of Medicine/Cardiology, David Geffen School of Medicine, 675 Charles E Young Dr. South, MRL-3579, Los Angeles, CA 90095

[2]Department of Surgery, David Geffen School of Medicine, 10833 Le Conte Avenue, 62-151 CHS, Los Angeles, CA 90095

[3]Los Angeles Biomedical Research Institute, Division of Urology at Harbor-UCLA Medical Center, 1124 West Carson Street, Torrance, CA 90502

[4]College of Textiles, North Carolina State University

[5]Department of Mechanical Engineering, Stevens Institute of Technology, 1 Castle Point on the Hudson, Carnegie 204, Hoboken, NJ 07030

[6]Department of Cardiothoracic Surgery, Stanford University Medical Center, 300 Pasteur Drive, Falk Bldg. CVRB; Stanford, CA 94305-5407

Abstract

Synthetic polymers or naturally-derived extracellular matrix (ECM) proteins have been used to create tissue engineering scaffolds; however, the need for surface modification in order to achieve polymer biocompatibility and the lack of biomechanical strength of constructs built using proteins alone remain major limitations. To overcome these obstacles, we developed novel hybrid constructs composed of both strong biosynthetic materials and natural human ECM proteins. Taking advantage of the ability of cells to produce their own ECM, human foreskin fibroblasts were grown on silicon-based nanostructures exhibiting various surface topographies that significantly enhanced ECM protein production. After 4 weeks, cell-derived sheets were harvested and histology, immunochemistry, biochemistry and multiphoton imaging revealed the presence of collagens, tropoelastin, fibronectin and glycosaminoglycans. Following decellularization, purified sheet-derived ECM proteins were mixed with poly(ε-caprolactone) to create fibrous scaffolds using electrospinning. These hybrid scaffolds exhibited excellent biomechanical properties with fiber and pore sizes that allowed attachment and migration of adipose tissue-derived stem cells. Our study represents an innovative approach to generate strong, non-cytotoxic scaffolds that could have broad applications in tissue regeneration strategies.

*To whom correspondence should be addressed: Katja Schenke-Layland, PhD, MSc, David Geffen School of Medicine at UCLA, Cardiovascular Research Laboratories, 675 Charles E Young Drive South, MRL-3579, Los Angeles, CA 90095, Phone: 310-206-6477, Fax: 310-206-5777, E-mail: kschenkelayland@mednet.ucla.edu.

Introduction

Today the concept of tissue engineering using cells incorporated into biodegradable scaffolds is being successfully applied to a variety of tissues including bone [1], cartilage [2], skin [3], blood vessels [4,5] and bladders [6]. The main approaches include the use of synthetic polymers or naturally derived components such as extracellular matrix (ECM) proteins [7,8]. One key concern regarding polymeric scaffolds is the inflammatory reaction that occurs upon their implantation and degradation [9]. While degradation can result in integration of the engineered tissue constructs, it can also cause damage to the cells seeded within the scaffolds or to the host cell-matrix environment. A second concern is the lack of biomechanical strength of constructs built using only natural proteins. The development of novel hybrid constructs composed of both strong biodegradable synthetic materials and natural, immunologically neutral ECM proteins might help to overcome the current obstacles [10].

Tissues and organs consist of specialized cells that are surrounded by ECM, which discloses the precise and site appropriate histoarchitecture. Typical cell harvest using enzymatic digestion results in separation of the ECM and cells, as well as disruption of both adhesive proteins and membrane receptors. In order to avoid enzymatic digestion, researchers have developed sheet-based concepts for the recreation of different tissues, using temperature-responsive culture surfaces [11], or have utilized cultured cells such as fibroblasts or smooth muscle cells for prolonged periods of time to induce production of sheets containing cells and their deposited ECM [12]. Cell signaling and metabolic cell activation can be affected by cell-surface interactions. The surfaces of biomaterials provide defined extracellular signals including surface chemistry, topography, charge, energy and wettability to the cells, which sense, communicate and respond to these signals [13]. Understanding the mechanisms by which cells sense and respond to chemical and physical signals from biomaterials will facilitate identification of novel biomaterial properties that control cell behavior [13]. New biomaterials, which can be reliably and rationally designed to interact with cells in a responsive manner, are very important to maintain appropriate cellular and molecular functions in culture. Exploiting biomimetic properties of biomaterials is an attractive strategy in developing novel cell-stimulating cues. One important consideration is the interaction of cells with nano-scale topographic interfaces *in vitro* and *in vivo*. Surface patterning might be an important issue in the formation and regulation of matrices for tissue engineering and implantable medical devices.

We have previously described that human foreskin fibroblasts adapted with an elongated and aligned morphology when cultured on surfaces with defined nano-patterns [13-15]. These growth patterns resembled a more natural state of fibroblasts *in vivo*, suggesting that the nano-patterned surface would be a more favorable substrate for the culture of these cells when compared to conventional flat bottom cell culture dishware. In this study, we have used the silicon-based nanostructures to instruct cells to produce ECM-containing sheets. We analyzed the matrix composition and structure of the sheets using routine histology, immunochemistry and biochemistry, as well as novel minimal-invasive multiphoton imaging technologies. We then decellularized the cell-derived sheets to obtain cell-free, purified ECM proteins for the generation of electrospun hybrid scaffolds that combined synthetic material with natural human sheet-ECM proteins to overcome limitations seen with scaffolds constructed with either one alone. We identified the properties of these novel scaffolds including fiber diameter, pore size and strength, and seeded the electrospun scaffolds with cells. Both, good biological and mechanical properties of the created hybrid scaffolds should prove useful for their application in the field of tissue engineering. Moreover, our innovative approach, taking advantage of the abundant synthesis of human ECM proteins *in vitro*, opens the possibility for the fabrication of custom-made, patient-specific scaffolds for regenerative medicine approaches.

Materials and Methods

Fabrication of nanostructures

Silicon nanostructures with superior control of pattern regularity were fabricated using interference lithography and deep reactive ion etching (DRIE) to create a surface topography with low, mid and high aspect ratios (ARs, ratio of height over width) as described before [16]. Sharp tips have been obtained by thermal oxidation followed by buffered oxide etching (BOE).

Cell culture on nanostructures

Human foreskin fibroblasts (HFFs, American Type Culture Collection (ATCC), Manassas, VA) were cultured in Dulbecco′s Modified Eagle Medium (DMEM, Invitrogen, Carlsbad, CA) supplemented with 10% FBS and penicillin/ streptomycin (100 U/ml, all Invitrogen), at 37°C and 5% CO_2. At confluence, HFFs were detached from the culture dishes using 0.05% trypsin/ EDTA followed by centrifugation at 1000 rpm for 5 minutes. To induce sheet formation, HFFs were re-suspended in culture medium and seeded at a density of 1×10^4 cells/cm^2 onto smooth control surfaces, as well as on nano-post (low, mid and high) and nano-grate (low, mid and high) samples. After culture for up to 4 weeks at 37°C and 5% CO_2, sheets formed on all surface structures that could be manually peeled off using a surgical tweezer.

Histological analysis and immunofluorescence staining

The harvested sheets were fixed immediately in 4% paraformaldehyde (Sigma-Aldrich, St. Louis, MO), followed by dehydration and embedding in paraffin. Semithin sections (5 μm) were cut and stained with hematoxylin and eosin (H&E) for general tissue development. To identify ECM formation, sections were stained using Movat's pentachrome and Picrosirius Red (0.1% Sirius Red in saturated picric acid) [17,18]. After histological staining, all sections were mounted using Entellan (Electron Microscopy Sciences, Hatfield, PA), analyzed and documented using routine bright-field light microscopy (Zeiss Axiovert 200 inverted microscope, Carl Zeiss MicroImaging Inc., Thornwood, NY). The Picrosirius Red stained sections were additionally analyzed by polarization microscopy using the Zeiss Axiovert 200 microscope combined with a polarizing filter (Carl Zeiss MicroImaging Inc.) [19]. Briefly, Sirius Red binds to collagen in a parallel fashion and enhances the normal birefringence of collagen fibers, which are then detectable as bright red or yellow fibers using polarization microscopy. In this way, also very thin fibrils that are undetectable using routine bright-field light microscopy become visible.

Immunofluorescence staining was performed to detect specific ECM proteins including collagen types I and IV, tropoelastin, fibronectin and decorin. Sections were permeabilized with 0.5% Triton X-100 (Sigma-Aldrich) for 10 min, followed by 3 washes with wash buffer (WB, PBS containing 0.1% Tween-20 (Sigma-Aldrich)). Non-specific antibody binding sites were blocked by incubating the samples for 30 minutes in blocking buffer (1% BSA, 2% goat serum and 0.5% Triton X-100 in PBS, all Sigma-Aldrich). Primary antibodies to collagen type I (1:50, Acris Antibodies GmbH, Herford, Germany), collagen type IV (1:100, abcam, Cambridge, MA), fibronectin (1:400, Dako, Carpinteria, CA), decorin (1:50, R&D Systems, Inc., Minneapolis, MN) and tropoelastin (1:100, abcam) were diluted in antibody buffer (PBS containing 1% BSA, 0.5% Triton X-100), and samples were then incubated for 60 minutes at room temperature, followed by several washes. Alexa Fluor 488-conjugated secondary antibodies (Molecular Probes, Eugene, OR) were applied to the samples and incubated for 30 minutes at room temperature. After several washes, the nuclei were stained with 4'-6-diamidino-2-phenylindole (DAPI, Sigma-Aldrich). Staining without primary antibodies served as controls. Digital images were acquired using a Leica DM IRB inverted microscope

system equipped with 20× (0.40 numerical aperture (NA)), 40× (0.75 NA) and 100× (1.25 NA) objectives (Leica Microsystems Inc., Bannockburn, IL).

Enzyme-linked immunosorbent assay (ELISA)

ELISA was used to determine collagen type I and decorin contents in the cell-derived ECM sheets according to the manufacturer's instructions (collagen type I, Cosmo Bio Co. LTD, Japan; decorin, R&D). Lysis buffer containing 20 mM Tris, 1% Triton X-100, 0.1% SDS, 1 mM NaF, 1 mM Na3VO4, 150 mM NaCl (all Sigma-Aldrich) and protease inhibitor cocktail (Boeringer Mannheim, Germany) was added to each sample. The detached sheets from each sample were homogenized by passing the lysate at least 5 times through a 20-gauge needle fitted to a syringe. This step was followed by centrifugation at 10,000 rpm at 4°C. The supernatant was transferred to a new tube. Total protein contents were measured using the Bradford method [20]. Equal amounts of protein from each time point (each 40 μg) were used for ELISA. A standard curve that was prepared from predetermined BSA standards. The absorbances of the samples were measured and the amounts of collagen type I and decorin were calculated based on a standard curve. Collagen type I and decorin contents were normalized to the total protein content and all values are expressed as μg (collagen type I) and pg (decorin) per mg protein.

Biochemical assays

Sheet homogenates were prepared as described above (see ELISA). Total collagen and glycosaminoglycan (GAG) contents were assessed using SIRCOL and BLYSCAN assays (Biocolor, Belfast, Northern Ireland) as per manufacturer's instructions. All contents were calculated relative to the total protein of the cell-derived sheets and are therefore expressed as μg per mg protein.

Sheet decellularization

Cell-derived sheets were decellularized using 0.25% sodium deoxycholate and 0.25% Triton X-100 (both Sigma-Aldrich) in a 6-hour incubation at 37°C under continuous shaking, followed by DNase (Qiagen, Valencia, CA) treatment and washing for 6 hours in PBS as described before [21]. Completeness of decellularization was evaluated with staining for nuclei using DAPI and H&E, and total DNA assessment using the PicoGreen assay (Invitrogen) as previously described [22,23].

After decellularization, cell-free ECM sheets were mechanically homogenized by pipetting up and down for several times. The sheet-derived homogenates were sequentially passed through a 20-gauge needle fitted to a syringe. This step was repeated at least five times, followed by high-speed vacuum centrifugation for 10 hours to remove water and dry the extracted samples. The dry weight of the samples was recorded, and total protein was determined using the Bradford method. For electrophoretic separation, sodium dodecyl sulfide-polyacrylamide gel electrophoresis (SDS-PAGE) was performed on a 10% gradient gel according to established protocols [24]. Separated proteins were stained for 1 hour with 0.4% Coomassie Brilliant Blue in 10% acetic acid (Sigma). Gels were de-stained in 10% acetic acid till the background was transparent.

Fabrication of electrospun scaffolds using sheet-derived ECM proteins

To fabricate scaffolds, the sheet-derived ECM protein extracts were dissolved in 1,1,1,3,3,3-hexafluoro-2-propanol (HFP) (125 μg protein/ml HFP). The HFP-dissolved protein alone or in combination with 10% poly(ε-caprolactone) (PCL) were then subtracted to electrospinning as described in detail before [10]. All electrospun scaffolds were subsequently analyzed using routine histology, SEM and multiphoton imaging.

Mechanical Testing

Electrospun samples were cut into 30 mm × 10 mm pieces for dynamic mechanical analysis (DMA). Initial monotonic tensile testing was conducted on one sample from the sheet-ECM proteins to establish a baseline testing point on an Instron MTS ReNew (Norwood, MA, USA) using a 250N load cell at a speed of 1 mm/ second and a gauge length of ~10 mm with a pneumatic flat jaw clamp. DMA testing was carried out on a DMA Q800 (TA Instruments, New Castle, Delaware, USA) using a strain sweep of 1 to 20 μm at a frequency of 1 Hz. Testing was carried out at 37°C using a thin film clamp with a gauge length of ~10 mm.

Multiphoton microscopy and SHG imaging

To determine the ECM produced by fibroblasts on each nanostructure and to identify the fiber composition in the electrospun scaffolds, multiphoton microscopy and SHG imaging were performed using a Zeiss LSM 510 META NLO femtosecond laser scanning system (Carl Zeiss MicoImaging Inc., Thornwood, NY), coupled to a software-tunable Coherent Chameleon titanium:sapphire laser (720 nm - 930 nm, 90 MHz; Coherent Laser Group, Santa Clara, CA, USA), and equipped with a high-resolution AxioCam HRc camera with 1300 × 1030 pixels (Carl Zeiss) as previously described [10,25,26]. Images were collected using an oil immersion Plan Apochromat 63×/1.4 NA objective lens (Carl Zeiss). Cellular and ECM structure-dependent autofluorescence and SHG were induced using wavelengths of 760 nm (cells, elastin) and 840 nm (collagen) as described [10,25,26]. Non-invasive serial optical horizontal sections of six different areas of each of the specimens were taken at four different depths (5, 15, 30 and 60 μm). To quantify and compare the intrinsic fluorescence signals of cells and ECM structures within the cell-produced sheets, lambda stacks were ascertained at emission wavelengths of 400 nm to 520 nm (in 10 nm increments) using the two-photon Chameleon laser tuned to an excitation wavelength of 840 nm. Emission was collected using the Zeiss META detector (spectral separator) of the LSM 510 Meta NLO system as previously described [26]. An E700SP filter (Chroma Technology, Brattleboro, VT) was installed in front of the detector to block UV radiation and to prevent scattered laser light from reaching the detector. SHG signals were collected through a 435 nm band pass filter. Signal intensities were reflected by the gray values of all the pixels within a region of interest (ROI) (gray value intensities (GVI). Mean intensities were calculated from peak intensities of the screened ROI areas. Accordingly, all results are presented as mean values ± standard deviations (SD).

Scanning electron microscopy (SEM)

All samples were rinsed with SEM buffer (0.1M sodium cacodylate buffer, pH 7.2, supplemented with 5% sucrose (all Sigma-Aldrich)), fixed for 30 minutes in 2% paraformaldehyde/ 2% glutaraldehyde and processed as previously described [10]. The samples were mounted onto stubs and sputter coated by gold/palladium (Au/Pd, thickness of ~10 nm) using Denton Desk II sputtering before scanning using JEOL JSM-6490 (JEOL USA, Inc. Peabody, MA) scanning electron microscope. Fiber diameters and pore sizes were measured on the scanning electron micrographs as described before [10].

Cell culture on electrospun scaffolds

Electrospun scaffolds were disinfected by immersion in 70% ethanol for 20 minutes followed by 3 × 5 minute rinses in sterile water and PBS. Human adipose-derived stem cells (hASCs) were prepared as described [27] and were seeded at passage 2 onto the electrospun scaffolds at a density of 10^6 cells/cm^2 to reach a confluent cell layer. The hASC-seeded scaffolds were then cultured for 4 weeks in DMEM-10% FBS at 37°C and 5% CO_2. To detect cell attachment as well as cell migration throughout the constructs, hASC-seeded scaffolds were evaluated with staining for nuclei using DAPI and H&E, and SEM as described above.

Statistics

All results are presented as mean values ± standard deviation (SD). Significant differences between the samples were assessed by analysis of variance and Fisher's PLSD (Tukey's) test and two-sided unpaired t-test, using significance at a p-value <0.05.

Results

Cell-nanostructure interactions

Two different patterns, nano-post (needle-like) and nano-grate (blade-like), were fabricated with three different ARs (Suppl. Fig. 1). ARs were systematically varied from low (50-100 nm in height), mid (200-300 nm) to high (500-600 nm), while the pattern periodicity (230 nm) and the tip sharpness (needle- or blade-like sharp tip) were retained in our samples as described before [13-15]. The efficiency of HFF attachment to polystyrene tissue culture dishware and smooth silicon surfaces was indistinguishable; therefore smooth silicon surfaces served as two-dimensional (2D) control surfaces in all our experiments. As previously described, HFFs exhibited distinct morphological features on surfaces with nano-post and nano-grate patterns [14]. In detail, cells that were cultured on 2D control surfaces with no patterns displayed a well-spread and flattened morphology. HFFs were elongated on nano-post samples with low and mid structures; however, with increasing height of the structures the cells showed poor adhesion, and on nano-post structures with high patterns only sparsely distributed cells with a round and small morphology and less cell-surface adhesions were detected. On the surfaces with nano-grate structures, the cells adapted with an elongated morphology and alignment along with the grate direction, which became more pronounced as the height of the nano-grates increased [14]. When cultured for up to 3 weeks, it had been shown that HFFs grown on these nanostructures induced the formation of cell-containing sheets [15].

Characterization of cell-derived ECM sheets

After 4 weeks in culture, cells formed sheets on all surface structures, comprising HFFs and HFF-produced ECM proteins (Suppl. Fig. 2). Movat pentachrome staining revealed the presence of ECM proteins such as collagens (yellow) and glycosaminoglycans (blue) in all sheets that were harvested from smooth control surfaces as well as from the different nanostructures (Fig. 1A). Double refraction (birefringence) was seen under polarized light in sections stained with Picrosirius Red, suggesting that fibrillar collagens had been deposited (Fig. 1B). Interestingly, it appeared that, specifically when focusing on the nano-grate high samples, the collagen fibers were aligned along the surface structures (Fig. 1B, n and Suppl. Fig. 3). The fibrillar nature of collagens was additionally confirmed using multiphoton-induced autofluorescence and SHG microscopy, although differences in the intrinsic fluorescence signal intensities, excited with wavelengths of 760 nm (cells and elastic structures) and 840 nm (collagen), were noted between the samples (Fig. 2). In detail, compared to weaker signals detected in samples derived from smooth control (Fig. 2A) and nano-post low, mid and high surfaces (Fig. 2B and C, a-c), robust autofluorescence and SHG signals were measured when excited with 840 nm in sheets obtained from nano-grate low, mid and high surfaces (Fig. 2B and C, d-f). Interestingly, we monitored significantly weaker cell intrinsic fluorescence patterns, specifically in the samples harvested from nano-post high surfaces when compared to smooth controls, nano-post low and mid, as well as all nano-grate surfaces. Superior cellular structures and a maximum cell autofluorescence were detected in the nano-grate high surfaces when excited with 760 nm (Fig. 2B, f and C, f). Additional immunofluorescence staining confirmed that the cell-derived sheet ECM contained fibrillar collagen type I and basement membrane type IV collagen, tropoelastin, fibronectin and decorin (Fig. 3).

To quantify the deposition of selected ECM proteins we performed biochemical assays and ELISA (Fig. 4). We detected significantly higher amounts of total GAG in the nano-grate mid

and high samples (mid: 23.9 ± 1.7 μg/mg; high: 24.1 ± 2.5 μg/mg) when compared to smooth controls (19.2 ± 1.4 μg/mg; $p = 0.0090$ (mid), $p = 0.0066$ (high)), nano-post low (20.5 ± 2.1 μg/mg; $p = 0.0453$ (mid), $p = 0.0334$ (high)), nano-post mid (20.2 ± 2.1 μg/mg; $p = 0.0337$; $p = 0.0247$ (high)) and nano-post high (12.1 ± 0.8 μg/mg; $p < 0.0001$ (mid and high)) samples (Fig. 4A). The total GAG content was significantly lower in nano-post high samples when compared to smooth controls ($p = 0.0004$) as well as nano-post low ($p < 0.0001$), nano-post mid ($p = 0.0001$), nano-grate low (21.7 ± 2.2 μg/mg; $p < 0.0001$) and nano-grate mid and high (both $p < 0.0001$) samples (Fig. 4A). Moreover, nano-post high samples displayed also significantly lower amounts of total collagen (13.1 ± 2.0 μg/mg) when compared to smooth controls (17.4 ± 0.2 μg/mg; $p = 0.0066$), nano-post low (18.4 ± 0.5 μg/mg; $p = 0.0014$), nano-post mid (19.2 ± 1.2 μg/mg; $p = 0.0004$), nano-grate low (17.6 ± 2.9 μg/mg; $p = 0.0046$), nano-grate mid (19.0 ± 1.9 μg/mg; $p = 0.0006$) and nano-grate high (19.4 ± 1.0 μg/mg; $p = 0.0003$) samples (Fig. 4A). ELISA revealed a significantly higher synthesis of collagen type I in nano-grate mid (15.9 ± 1.1 μg/mg) and nano-grate high (15.5 ± 0.3 μg/mg) samples when compared to nano-post mid (14.2 ± 0.1 μg/mg; $p = 0.0276$ (mid), $p = 0.0488$ (high)) and nano-post high (13.1 ± 1.1 μg/mg; $p = 0.0029$ (mid), $p = 0.0093$ (high)) specimens (Fig. 4B). No significant differences in deposition of decorin were detected (7.6 ± 0.2 pg/mg smooth, 7.4 ± 0.2 pg/mg nano-post low, 7.7 ± 0.1 pg/mg nano-post mid, 7.6 ± 0.2 pg/mg nano-post high, 7.8 ± 0.5 pg/mg nano-grate low, 7.9 ± 0.6 pg/mg nano-post mid, 7.8 ± 0.4 pg/mg nano-post high; all $p > 0.05$) (Fig. 4C).

Electrospinning of sheet-derived proteins and PCL

To obtain cell-free, purified ECM proteins, we exposed the cell-derived sheets to 0.25% sodium deoxycholate and 0.25% Triton X-100, followed by DNase treatment according to an established protocol [21]. As assessed by DAPI and H&E staining, the decellularization procedure resulted in an almost complete loss of all cellular structures within the sheets (Fig. 5A). DNA assays confirmed these results showing a significantly decreased DNA content in the decellularized samples when compared to non-treated controls (402 ± 43 ng/mg dry weight in controls versus 14 ± 6 ng/mg dry weight in treated samples) (Fig. 5B). Following decellularization and subsequent high-speed vacuum centrifugation, SDS-PAGE revealed the presence of intact proteins in the sheet-ECM extracts (Fig. 5C). The purified ECM proteins were then used for scaffold fabrication employing electrospinning technologies. In order to avoid the need for cross-linking agents such as glutaraldehyde, sheet-ECM proteins were stabilized using the biopolymers PCL [10]. Sheet-ECM proteins as well as 10% PCL were dissolvable in HFP and were electrospinnable, either separately or when mixed together. SEM analysis of the electrospun sheet-ECM and mixtures of sheet-ECM with 10% PCL showed the presence of a 3D fibrous mat with fibers in random orientation (Fig. 6A, **a** and **c-e**). In contrast, electrospinning of 10% PCL alone resulted in non-fibrous constructs (Fig. 6A, **b**). Multiphoton-induced autofluorescence imaging confirmed the SEM data and revealed further that the fibers seen in the sheet-ECM/PCL scaffolds represented mainly a hybrid of the base materials (Fig. 6B).

Fiber diameter, pore size and mechanical properties of hybrid scaffolds

The average fiber diameter, pore size and mechanical properties of the various scaffolds are summarized in Table 1. As shown, there were no significant differences between the average fiber size of sheet-ECM/PCL (0.37 ± 0.07 μm) compared to electrospun sheet-ECM proteins alone (0.32 ± 0.05 μm). In contrast, the average pore size was significantly smaller in the electrospun sheet-ECM/PCL scaffolds (32.24 ± 0.96 μm^2) when compared to electrospun sheet-ECM scaffolds (45.71 ± 0.98 μm^2). DMA revealed further that both scaffolds made of either sheet-ECM alone or sheet-ECM and PCL in combination exhibited extreme brittleness and broke when placed into the clamp for DMA testing. However, the sheet-ECM scaffolds showed a greater amount of elasticity during the course of the testing protocol (Fig. 7). In

contrast, the sheet-ECM/PCL scaffolds were able to withstand a higher amount of stress compared to the samples made of just ECM proteins. For higher amounts of amplitude during the strain sweep (> 20 μm), the sheet-ECM scaffolds had a storage modulus of 2.94 ± 0.96 MPa, while the sheet-ECM/PCL constructs had a significantly higher storage modulus of 7.92 ± 1.61 MPa (Fig. 7A). However, the sheet-ECM/PCL constructs exhibited also a significantly higher loss modulus as displayed in Figure 7B (loss modulus values at the higher amplitude = 0.24 ± 0.30 MPa (sheet-ECM) versus 0.75 ± 0.46 MPa (sheet-ECM/PCL)), indicating that the sheet-ECM/PCL scaffolds are able to withstand high amounts of strain, but are unable to do so cyclically. It also reflects the extreme brittle characteristics of these scaffolds and quantitatively suggests that there is little elasticity present. Tan δ values represent the relationship between the storage and loss moduli and are indicative for the ability of the sample to recover from deformation. At higher amounts of strain, the sheet-ECM samples had a Tan δ value of 0.081 ± 0.055 compared to 0.096 ± 0.017 in the sheet-ECM/PCL hybrid scaffolds (Fig. 7C). We noted a gradual increase in the Tan δ values as the strain sweep progressed and the amplitude increased, indicating that the scaffold's ability to recover from the deformation of the strain is beginning to weaken and eventually the scaffold will rupture. This increase was seen at a relatively low amount of strain, indicating that there is sufficient strength in the scaffold, but little to no elasticity.

hASC response to electrospun hybrid scaffolds

Although we could successfully electrospin pure sheet-ECM proteins into fibrous mats, these scaffolds dissolved and lost their 3D structure when introduced into aqueous conditions (cell culture medium). To study cell-scaffold interactions we used therefore the hybrid scaffolds composed of sheet-ECM and 10% PCL, seeded them using hASCs, and culture the constructs for 4 weeks. No surface modification of the electrospun scaffolds was necessary to ensure attachment of hASCs. SEM of the cell-seeded hybrid scaffolds revealed cell attachment and confluent coverage of the entire scaffold surface (Fig. 8A). H&E and DAPI staining confirmed this result (Fig. 8B, C). Moreover, using the LSM 510 Meta NLO imaging system, non-invasive serial optical horizontal sections (z-stacks) of the DAPI-stained scaffolds demonstrated robust cell migration throughout the entire scaffold (Fig. 8C).

Discussion

There is an obvious necessity to improve traditional treatments for cardiovascular diseases and develop alternatives to current organ transplantation therapies. An alternative approach is to design tissue-engineered constructs. The field of cardiovascular tissue engineering has attempted to produce clinically viable conduits such as blood vessels and heart valves by using a variety of *in vitro* approaches that typically combine living cells seeded onto biomimetic scaffolds [4,5,28-36]. One aspect of tissue engineering has been the design of scaffolds with specific mechanical and biological properties similar to the native extracellular environment in order to modulate cellular behavior. The intricate complexities of this spatial and temporal environment dynamically influence phenotypic and other cellular behavior by providing indirect and direct informational signaling cues [8,25,37-39]. Interactions between cells and ECM can modulate cellular activities such as migration, proliferation, differentiation, gene expression and secretion of various growth factors and cytokines. Thus, the more closely the *in vivo* environment can be recreated, the more likely is the success of the tissue engineering effort [13,40-42].

In the present study, we have cultured human fibroblasts on smooth control surfaces and silicon-based nanostructures exhibiting various surface topographies to determine their ability to instruct cells to produce ECM-containing sheets. We further compared the quality of the obtained ECM proteins and quantified ECM production. After 4 weeks in culture, the

fibroblasts formed a robust sheet on all surfaces containing their own ECM proteins including collagens, tropoelastin, fibronectin and various glycosaminoglycans. Interestingly, we found that culture on especially the nano-grate structures with mid to high patterns resulted in a significant increase in ECM protein production; however, in order to be able to upscale the *in vitro* production of human ECM proteins, further improvement of the nanostructure technology (size of the structures and surface topography) will be necessary.

We could successfully isolate, purify and electrospin the sheet-derived ECM proteins in order to fabricate custom-made scaffolds, suitable for different tissue engineering applications. Although we could successfully electrospin pure sheet-ECM proteins into fibrous mats, these scaffolds dissolved and lost their 3D structure when introduced into cell culture medium without the use of any cross-linking reagent or other stabilizing additive. As demonstrated by our previous work, exposing the electrospun scaffolds to a cross-linker such as glutaraldehyde, intermolecularly cross-links the scaffolds, making cell-culturing possible; however, the use of glutaraldehyde also reduces porosity dramatically [10], and glutaraldehyde-treated biomaterials can be cytotoxic [43]. Moreover, results from clinical studies have shown that treatment with glutaraldehyde can cause vascular graft failure related to aneurysm formation, calcification and infection [44-46]. In order to avoid the need for cross-linking agents, sheet-ECM proteins were stabilized using PCL. PCL is a Food and Drug Administration (FDA) approved material that is already clinically used as drug delivery device and suture material (sold under the brand name Monocryl or generically) [47,48]. Although electrospinning of PCL alone resulted in an amorphous/non-fibrous suboptimal scaffold, adding PCL to the sheet-derived ECM proteins instead of a chemical cross-linking reagent not only reduces the potential toxic problem, but this approach also produced a novel biomaterial with improved mechanical and biological properties. Furthermore, it is known that cell adhesion to pure synthetic polymers is poor due to the lack of specific cell-binding sites and therefore requires additional modifications [49-52]. By combining cell-produced ECM proteins with PCL prior to electrospinning, cell attachment onto the fibers in the presented hybrid scaffolds was possible without further surface modification. The sheet-ECM/PCL hybrid scaffolds clearly supported attachment and proliferation of hASCs as well as cell migration throughout the scaffold. It is likely that the gradual degradation of PCL in the hybrid scaffold creates more space for cell migration and that cell-produced ECM proteins provide specific binding sites for further cellular attachment and proliferation.

The mechanical properties of a scaffold are an important design parameter for maintaining stability before the cells produce their own ECM [53,54]. Here we used novel dynamic mechanical testing to evaluate the scaffolds' potential use in dynamic strain environments. Under the determined protocol for DMA testing, the scaffolds were strained under increasing increments and allowed to recover fully at 37°C, until testing concluded or permanent deformation occurred. DMA testing determines both the storage and loss moduli and calculates the ratio between the two and the Tan δ value. The two moduli indicate the elastic properties of the scaffolds and their ability to recover from such strain over time [55-57]. Specifically, the storage modulus measures the amount of stored energy, corresponding to the elastic portion of the scaffold. The loss modulus is the expression of the energy lost to molecular rearrangement or dissipated as heat, representing the viscous portion of the material and its ability to recover from permanent deformation. The Tan δ values further examine the relationship between the storage and loss moduli of the material, by representing the ratio of the storage modulus to the loss modulus as the strain steadily increases [55-57]. In our study, we found that the Tan δ curve gradually increased and that the elastic nature of the sheet-ECM/PCL hybrid scaffolds decreased. As the strain increased, the fibers were allowed more surface area to align and recover from such strain. As the loss modulus increased, the scaffolds' ability to recover from repetitive strain decreased. Here we see both the storage and the loss modulus increased, causing the subsequent Tan δ values to increase. This correlates to the gradual loss

of elasticity observed when the scaffolds were physically handled and subjected to dynamic loading conditions. This relationship allows us to determine the best amplitude and amount of strain and stress that our scaffolds can withstand. Interestingly, we found that the sheet-ECM scaffolds were only able to withstand a small degree of stress while showing superior elasticity due to less viscous loss. In contrast, the more stable, but relatively less elastic sheet-ECM/PCL hybrid scaffolds exhibited a higher degree of viscous dissipation.

In summary, the human fibroblast-derived ECM protein/PCL hybrid scaffolds showed sufficient tensile strength while supporting cellular proliferation and migration into the scaffold. This unique ability might help to overcome current obstacles, bringing the hybrid scaffolds closer to a clinical realization.

Conclusions

Native ECM is comprised of a complex network of structural and regulatory proteins that are arrayed into a tissue-specific, biomechanically optimal, fibrous matrix. The multifunctional nature of the native ECM will need to be considered in the design and fabrication of tissue-engineering scaffolds. Here we introduced a novel concept to generate human ECM proteins *in vitro*. We further fabricated human ECM/PCL electrospun hybrid scaffolds with favorable mechanical properties and binding sites for cell attachment and proliferation. We believe that electrospinning using a combination of strong biopolymers and natural, potentially patient-specific proteins better recapitulates key features of native ECM substrates while providing superior mechanical and biochemical properties. Ease of *in vitro* generation of autologous human ECM proteins and the combination with electrospinning technologies will make this method valuable for clinical applications in regenerative medicine.

Supplementary Material

Refer to Web version on PubMed Central for supplementary material.

Acknowledgments

The authors would like to thank Prof. Chang-Jin Kim (Department of Mechanical and Aerospace Engineering, UCLA) for providing the nanostructures. This work was supported by the NIH (5T32HL007895-10 (K.S-L.) and the Department of Surgery at UCLA. Confocal laser scanning microscopy was performed at the CNSI Advanced Light Microscopy/Spectroscopy Shared Resource Facility at UCLA, supported with funding from NIH-NCRR shared resources grant (CJX1-443835-WS-29646) and NSF Major Research Instrumentation grant (CHE-0722519).

References

1. Vacanti CA, Bonassar LJ, Vacanti MP, Shufflebarger J. Replacement of an avulsed phalanx with tissue-engineered bone. N Engl J Med 2001;344(20):1511–4. [PubMed: 11357154]
2. Marcacci M, Berruto M, Brocchetta D, Delcogliano A, Ghinelli D, Gobbi A, et al. Articular cartilage engineering with Hyalograft C: 3-year clinical results. Clin Orthop Relat Res 2005;(435):96–105. [PubMed: 15930926]
3. Charruyer A, Ghadially R. Stem cells and tissue-engineered skin. Skin Pharmacol Physiol 2009;22(2): 55–62. [PubMed: 19188753]
4. Poh M, Boyer M, Solan A, Dahl S, Pedrotty D, Banik S, et al. Blood vessels engineered from human cells. Lancet 2005;365(9477):2122–4. [PubMed: 15964449]
5. Shinoka T, Imai Y, Ikada Y. Transplantation of a tissue-engineered pulmonary artery. N Engl J Med 2001;344(7):532–3. [PubMed: 11221621]
6. Atala A, Bauer SB, Soker S, Yoo JJ, Retik AB. Tissue engineered autologous bladders for patients needing cystoplasty. Lancet 2006;367(9518):1241–6. [PubMed: 16631879]

7. Chung HJ, Park TG. Surface engineered and drug releasing pre-fabricated scaffolds for tissue engineering. Adv Drug Deliv Rev 2007;59(45):249–262. [PubMed: 17482310]
8. Badylak SF, Freytes DO, Gilbert TW. Extracellular matrix as a biological scaffold material: Structure and function. Acta Biomater 2009;5(1):1–13. [PubMed: 18938117]
9. Mikos AG, McIntire LV, Anderson JM, Babensee JE. Host response to tissue engineered devices. Adv Drug Deliv Rev 1998;33(12):111–139. [PubMed: 10837656]
10. Heydarkhan-Hagvall S, Schenke-Layland K, Dhanasopon AP, Rofail F, Smith H, Wu BM, et al. Three-dimensional electrospun ECM-based hybrid scaffolds for cardiovascular tissue engineering. Biomaterials 2008;29(19):2907–14. [PubMed: 18403012]
11. Yang J, Yamato M, Shimizu T, Sekine H, Ohashi K, Kanzaki M, et al. Reconstruction of functional tissues with cell sheet engineering. Biomaterials 2007;28(34):5033–43. [PubMed: 17761277]
12. L'Heureux N, Dusserre N, Konig G, Victor B, Keire P, Wight TN, et al. Human tissue-engineered blood vessels for adult arterial revascularization. Nat Med 2006;12(3):361–5. [PubMed: 16491087]
13. Heydarkhan-Hagvall S, Choi CH, Dunn J, Heydarkhan S, Schenke-Layland K, MacLellan WR, et al. Influence of Systematically Varied Nano-Scale Topography on Cell Morphology and Adhesion. Cell Communication and Adhesion 2007;14:181–194. [PubMed: 18163229]
14. Choi CH, Hagvall SH, Wu BM, Dunn JC, Beygui RE, Kim CJ. Cell interaction with three-dimensional sharp-tip nanotopography. Biomaterials 2007;28(9):1672–9. [PubMed: 17174392]
15. Choi CH, Heydarkhan-Hagvall S, Wu BM, Dunn JC, Beygui RE, Kim CJ. Cell growth as a sheet on three-dimensional sharp-tip nanostructures. J Biomed Mater Res A. 2008 June;(3)in press
16. Choi CH, Kim CJ. Fabrication of dense array of high-aspect-ratio nanostructures over a large sample area with sidewall profile and tip sharpness control. Nanotechnology 2006;17:5326–33.
17. Schenke-Layland K, Xie J, Angelis E, Starcher B, Wu K, Riemann I, et al. Increased degradation of extracellular matrix structures of lacrimal glands implicated in the pathogenesis of Sjögren's syndrome. Matrix Biol 2008;27(1):53–66. [PubMed: 17689946]
18. Junqueira LC, Bignolas G, Brentani RR. Picrosirius staining plus polarization microscopy, a specific method for collagen detection in tissue sections. Histochem J 1979;11(4):447–55. [PubMed: 91593]
19. Mol A, van Lieshout MI, Dam-de Veen CG, Neuenschwander S, Hoerstrup SP, Baaijens FP, et al. Fibrin as a cell carrier in cardiovascular tissue engineering applications. Biomaterials 2005;26(16): 3113–21. [PubMed: 15603806]
20. Bradford MM. A rapid and sensitive method for the quantitation of microgram quantities of protein utilizing the principle of protein-dye binding. Anal Biochem 1976;7(72):248–54. [PubMed: 942051]
21. Rieder E, Kasimir MT, Silberhumer G, Seebacher G, Wolner E, Simon P, et al. Decellularization protocols of porcine heart valves differ importantly in efficiency of cell removal and susceptibility of the matrix to recellularization with human vascular cells. J Thorac Cardiovasc Surg 2004;127(2): 399–405. [PubMed: 14762347]
22. Gilbert TW, Freundb SJM, Badylak SF. Quantification of DNA in Biologic Scaffold Materials. J Surg Res. 2008 March;(13)in press
23. Schenke-Layland K, Vasilevski O, Opitz F, König K, Riemann I, Halbhuber KJ, et al. Impact of decellularization of xenogeneic tissue on extracellular matrix integrity for tissue engineering of heart valves. J Struct Biol 2003;143(3):201–8. [PubMed: 14572475]
24. Schenke-Layland K, Riemann I, Opitz F, König K, Halbhuber KJ, Stock UA. Comparative study of cellular and extracellular matrix composition of native and tissue engineered heart valves. Matrix Biol 2004;23(2):113–25. [PubMed: 15246110]
25. Schenke-Layland K. Non-invasive multiphoton imaging of extracellular matrix structures. J Biophoton 2008;1(6):451–62.
26. Schenke-Layland K, Xie J, Heydarkhan-Hagvall S, Hamm-Alvarez SF, Stock UA, Brockbank KGM, et al. Optimized Preservation of Extracellular Matrix in Cardiac Tissues: Implications for Long-Term Graft Durability. Ann Thorac Surg 2007;83(5):1641–50. [PubMed: 17462373]
27. Heydarkhan-Hagvall S, Schenke-Layland K, Yang JQ, Heydarkhan S, Xu Y, Zuk P, et al. Human adipose stem cells: a potential cell source for cardiovascular tissue engineering. Cells Tissues Organs 2008;187(4):263–74. [PubMed: 18196894]
28. Weinberg CB, Bell E. A blood vessel model constructed from collagen and cultured vascular cells. Science 1987;231:397–400. [PubMed: 2934816]

29. Schenke-Layland K, Opitz F, Gross M, Döring C, Halbhuber KJ, Schirrmeister F, et al. Complete dynamic repopulation of decellularized heart valves by application of defined physical signals-an in vitro study. Cardiovasc Res 2003;60(3):497–509. [PubMed: 14659795]
30. Torikai K, Ichikawa H, Hirakawa K, Matsumiya G, Kuratani T, Iwai S, et al. A self-renewing, tissue-engineered vascular graft for arterial reconstruction. J Thorac Cardiovasc Surg 2008;136(1):37–45. [PubMed: 18603051]
31. Rashid ST, Fuller B, Hamilton G, Seifalian AM. Tissue engineering of a hybrid bypass graft for coronary and lower limb bypass surgery. FASEB J 2008;22(6):2084–9. [PubMed: 18203957]
32. Robinson PS, Johnson SL, Evans MC, Barocas VH, Tranquillo RT. Functional tissue-engineered valves from cell-remodeled fibrin with commissural alignment of cell-produced collagen. Tissue Eng Part A 2008;14(1):83–95. [PubMed: 18333807]
33. Kasyanov VA, Hodde J, Hiles MC, Eisenberg C, Eisenberg L, De Castro LE, et al. Rapid biofabrication of tubular tissue constructs by centrifugal casting in a decellularized natural scaffold with laser-machined micropores. J Mater Sci Mater Med 2009;20(1):329–37. [PubMed: 18807150]
34. Zhang X, Wang X, Keshav V, Wang X, Johanas JT, Leisk GG, et al. Dynamic culture conditions to generate silk-based tissue-engineered vascular grafts. Biomaterials. 2009 Feb 19;in press
35. Nieponice A, Soletti L, Guan J, Deasy BM, Huard J, Wagner WR, et al. Development of a tissue-engineered vascular graft combining a biodegradable scaffold, muscle-derived stem cells and a rotational vacuum seeding technique. Biomaterials 2008;29(7):825–33. [PubMed: 18035412]
36. Hong H, Dong GN, Shi WJ, Chen S, Guo C, Hu P. Fabrication of biomatrix/polymer hybrid scaffold for heart valve tissue engineering in vitro. ASAIO J 2008;54(6):627–32. [PubMed: 19033778]
37. Hutmacher DW. Scaffold design and fabrication technologies for engineering tissues--state of the art and future perspectives. J Biomater Sci Polym Ed 2001;12(1):107–24. [PubMed: 11334185]
38. Chan G, Mooney DJ. New materials for tissue engineering: towards greater control over the biological response. Trends Biotechnol 2008;26(7):382–92. [PubMed: 18501452]
39. Ngangan AV, McDevitt TC. Acellularization of embryoid bodies via physical disruption methods. Biomaterials 2009;30(6):1143–9. [PubMed: 19042017]
40. Li WJ, Laurencin CT, Caterson EJ, Tuan RS, Ko FK. Electrospun nanofibrous structure: a novel scaffold for tissue engineering. J Biomed Mater Res 2002;60:613–21. [PubMed: 11948520]
41. Mo XM, Xu CY, Kotaki M, Ramakrishna S. Electrospun P(LLA-CL) nanofiber: a biomimetic extracellular matrix for smooth muscle cell and endothelial cell proliferation. Biomaterials 2004;25 (10):1883–90. [PubMed: 14738852]
42. Smith LA, Ma PX. Nano-fibrous scaffolds for tissue engineering. Colloids and Surfaces B: Biointerfaces 2004;39:125–31.
43. van Wachem PB, van Luyn MJ, Olde Damink LH, Dijkstra PJ, Feijen J, Nieuwenhuis P. Biocompatibility and tissue regenerating capacity of cross-linked dermal sheep collagen. J Biomed Mater Res 1994;28(3):353–6. [PubMed: 8077250]
44. Clarke DR, Lust RM, Sun YS, Black KS, Ollerenshaw JD. Transformation of nonvascular acellular tissue matrices into durable vascular conduits. Ann Thorac Surg 2001;71(5):433–36.
45. Field PL. The chemically treated bovine ureter-clinical performance of a novel biological vascular prosthesis. Cardiovasc Surg 2003;11(1):30–4. [PubMed: 12543569]
46. Widmer MK, Aregger F, Stauffer E, Savolainen H, Heller G, Hakki H, et al. Intermediate outcome and risk factor assessment of bovine vascular heterografts used as AV-fistulas for hemodialysis access. Eur J Vasc Endovasc Surg 2004;27(6):660–5. [PubMed: 15121120]
47. Luciani A, Coccoli V, Orsi S, Ambrosio L, Netti PA. PCL microspheres based functional scaffolds by bottom-up approach with predefined microstructural properties and release profiles. Biomaterials 2008;29(36):4800–7. [PubMed: 18834628]
48. Zalfen AM, Nizet D, Jérôme C, Jérôme R, Frankenne F, Foidart JM, et al. Controlled release of drugs from multi-component biomaterials. Acta Biomater 2008;4(6):1788–96. [PubMed: 18583206]
49. Smetana K Jr. Cell biology of hydrogels. Biomaterials 1993;14(14):1046–50. [PubMed: 8312457]
50. Boyan BD, Hummert TW, Dean DD, Schwartz Z. Role of material surfaces in regulating bone and cartilage cell response. Biomaterials 1996;17(2):137–46. [PubMed: 8624390]

51. Nikolovski J, Mooney D. Smooth muscle cell adhesion to tissue engineering scaffolds. Biomaterials 2000;21(20):2025–32. [PubMed: 10966011]

52. Woo KM, Chen VJ, Ma PX. Nano-fibrous scaffolding architecture selectively enhances protein adsorption contributing to cell attachment. J Biomed Mater Res A 2003;67(2):531–7. [PubMed: 14566795]

53. Discher DE, Janmey P, Wang YL. Tissue cells feel and respond to the stiffness of their substrate. Science 2005;310(5751):1139–43. [PubMed: 16293750]

54. Yeung T, Georges PC, Flanagan LA, Marg B, Ortiz M, Funaki M, et al. Effects of substrate stiffness on cell morphology, cytoskeletal structure, and adhesion. Cell Motil Cytoskeleton 2005;60:24–35. [PubMed: 15573414]

55. Bhushan B, Ma T, Higashioji T. Tensile and dynamic mechanical properties of improved ultrathin polymeric films. J Applied Polymer Science 2001;83(10):2225–44.

56. Boyaud MF, Ait-Kadi A, Bousmina M, Michael A, Cassagnau P. Organic short fibre/thermoplastic composites: morphology and thermorheological analysis. Polymer 2001;42:6515–26.

57. Menard, KP. Dynamic Mechanical Analysis: A Practical Introduction. Vol. 2nd. CRC Press; 2008. p. 1-188.

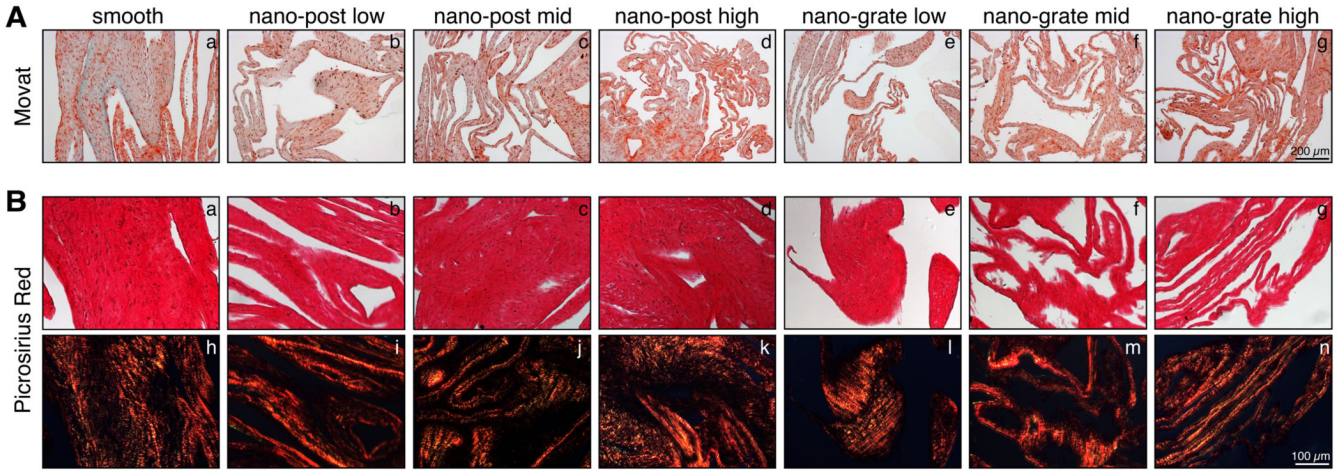

Figure 1.

(**A**) Movat pentachrome stained sections of sheets derived from HFFs that were cultured on smooth control (**a**), nano-post low (**b**), nano-post low (**c**), nano-post high (**d**), nano-grate low (**e**), nano-grate mid (**f**), and nano-grate high (**g**) surfaces. Scale bar equals 200 μm. (**B**) Picrosirius Red staining of smooth control (**a**), nano-post low (**b**), nano-post low (**c**), nano-post high (**d**), nano-grate low (**e**), nano-grate mid (**f**), and nano-grate high (**g**) surface-derived sheets with the corresponding polarization microscopic images (smooth control (**h**), nano-post low (**i**), nano-post low (**j**), nano-post high (**k**), nano-grate low (**l**), nano-grate mid (**m**), and nano-grate high (**n**) surfaces). Scale bar equals 100 μm.

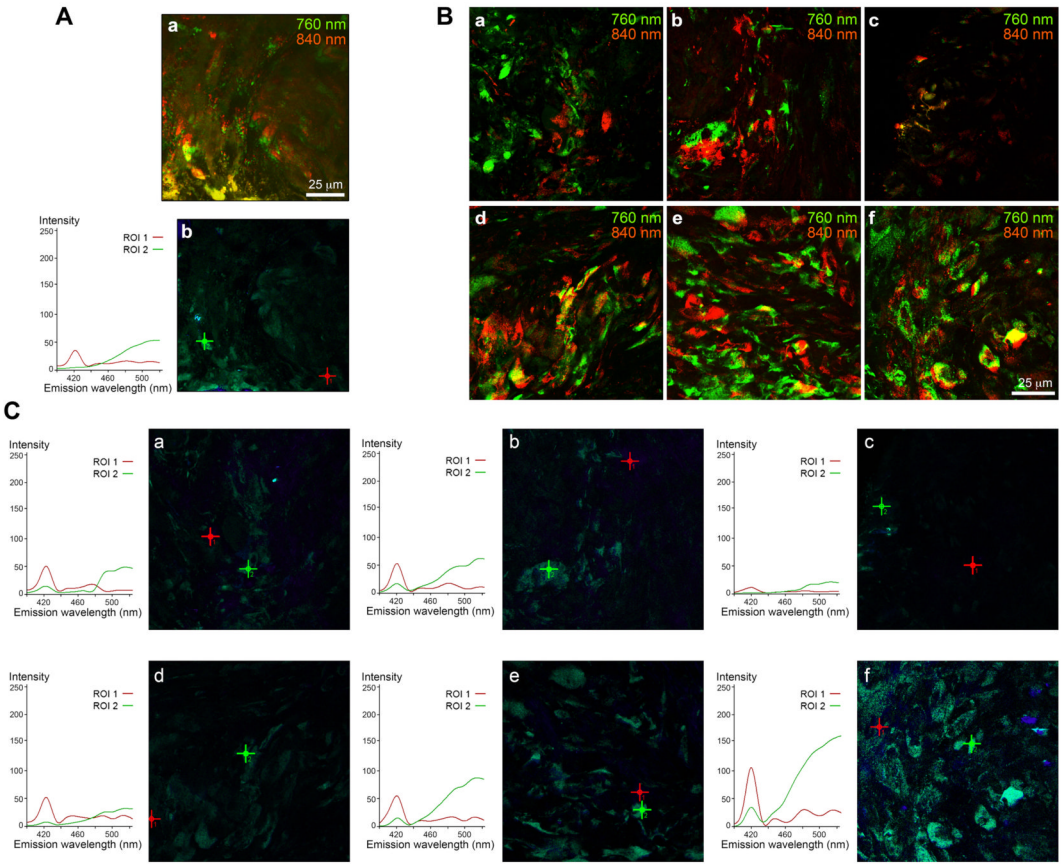

Figure 2.

Multiphoton-induced autofluorescence imaging (**A**, **a** and **B**) and SHG signal profiling (**A**, **b** and **C**) of sheets grown on smooth control (**A**), nano-post low, mid and high (**B, a-c** and **C, a-c**), as well as nano-grate low, mid and high (**B, d-f** and **C, d-f**) surfaces. (**A**, **a; B**) Cells and elastic structures are depicted using an excitation wavelength of 760 nm (green) and collagen fibers are visualized using an excitation wavelength of 840 nm (red). (**A**, **b; C**) The graphs represent peak signal intensities of collagenous fibers (ROI 1, red) and cells and elastic structures (ROI 2, green) shown in the corresponding lambda stack overlay images, depicted by the red (ROI 1) or the green cross (ROI 2). Scale bars equal 25 μm.

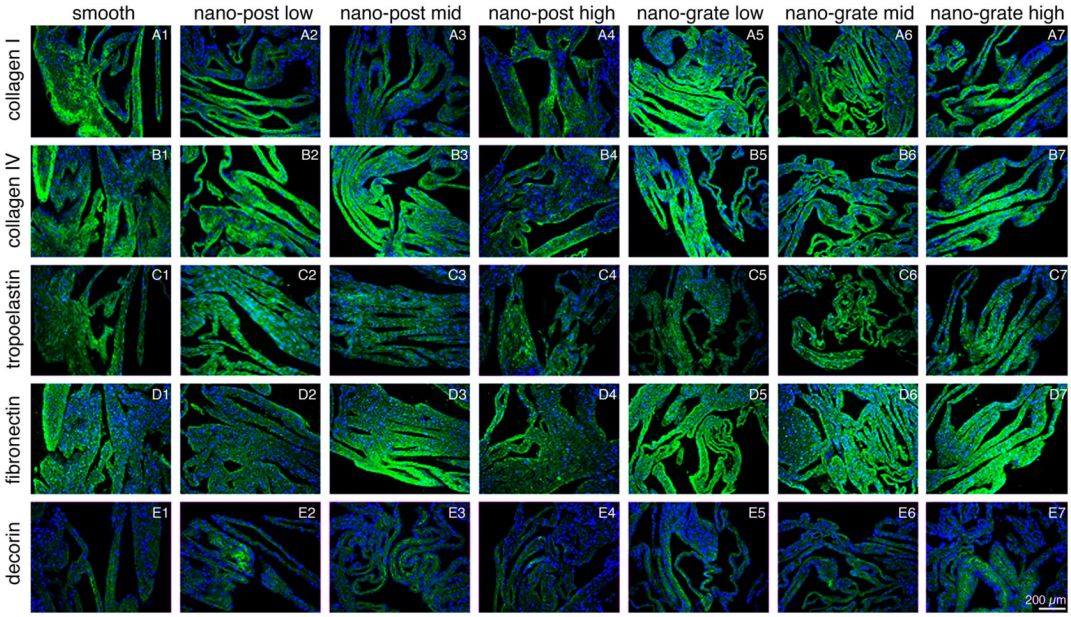

Figure 3.

Immunolabeling of sheets derived from smooth control (**A1-E1**), nano-post low (**A2-E2**), nano-post mid (**A3-E3**), nano-post high (**A4-E4**), nano-grate low (**A5-E5**), nano-grate mid (**A6-E6**) and nano-grate high (**A7-E7**) surfaces identifies expression for collagen types I and IV (**A1-7** and **B1-7**), tropoelastin (**C1-7**), fibronectin (**D1-7**) and decorin (**E1-7**) (all green). Cell nuclei are stained with DAPI (blue). Scale bar equals 200 μm.

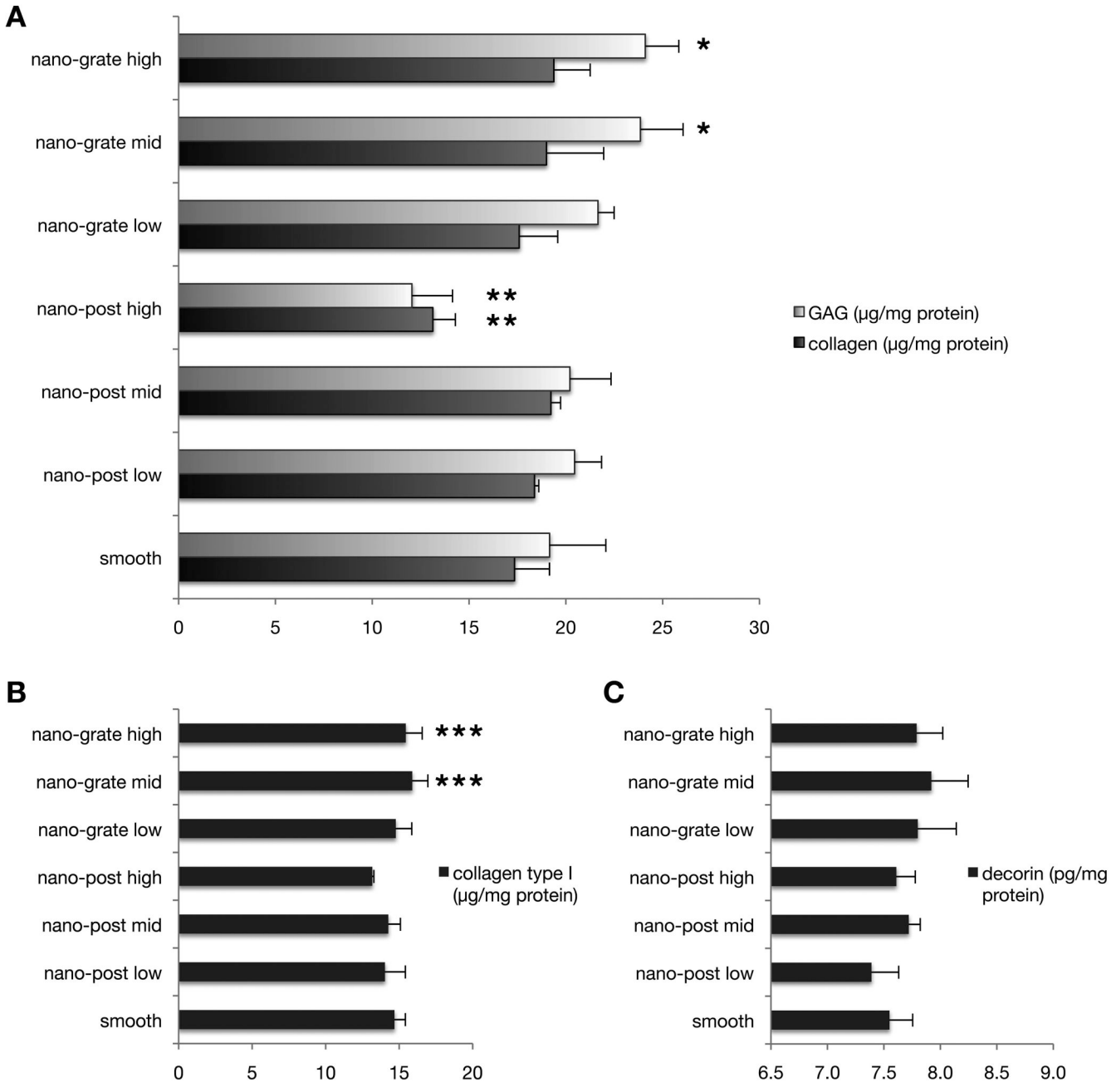

Figure 4.

Biochemical assays (**A**) and ELISA analyses (**B** and **C**) reveal significantly higher ECM protein depositions in sheets that had been harvested from nano-grate surfaces. (**A**) *$p < 0.05$ increased against smooth, nano-post low, mid and high; **$p < 0.05$ GAG decreased against smooth, nano-post low and mid, nano-grate low, mid and high; (**B**) ***$p < 0.05$ increased against nano-post mid and high.

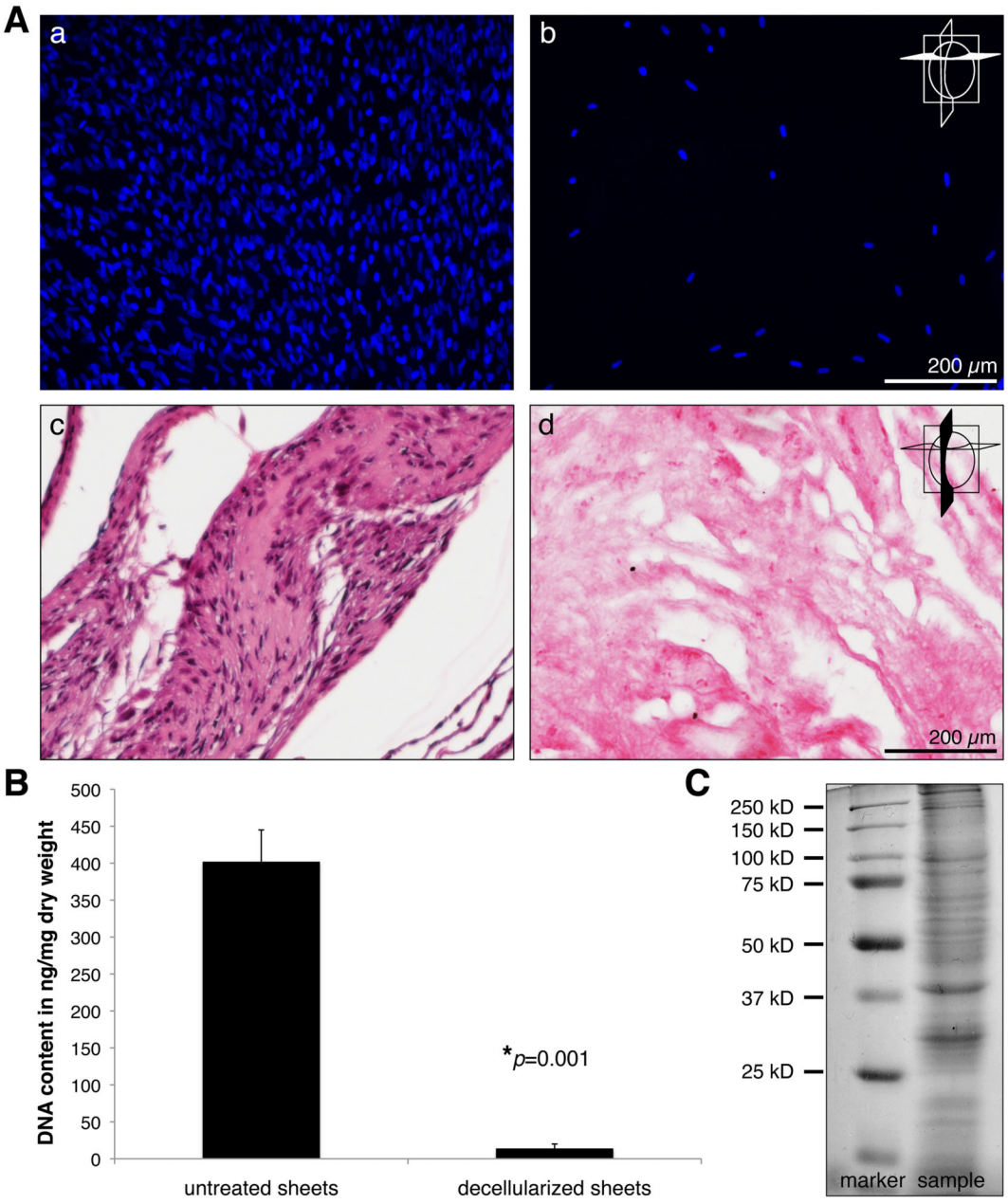

Figure 5.

(**A**) Untreated control sheets (**a**, **c**) and decellularized sheets (**b**, **d**) were evaluated with staining for nuclei using DAPI (**a**, **b**; cross section) and H&E (**c**, **d**; longitudinal section). Scale bars equal 200 μm. (**B**) An almost complete removal of cells in the decellularized sheets was also supported by DNA assays. (**C**) SDS-PAGE of cell-free, extracted, sheet-derived ECM reveals the presence of intact proteins.

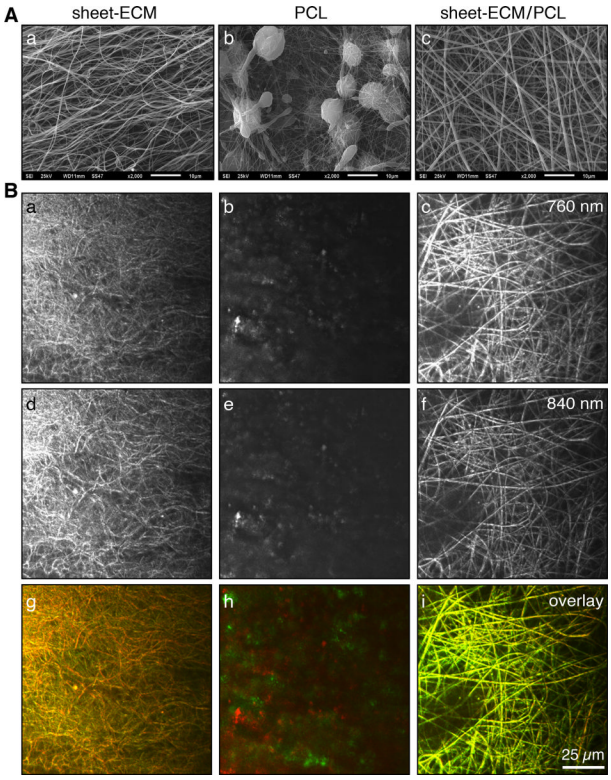

Figure 6.

(**A**) Scanning electron micrographs of electrospun scaffolds composed of sheet-ECM (**a**), PCL (**b**) and sheet-ECM in combination with PCL (**c**). Scale bars equal 10 μm. (**B**) Multiphoton-induced autofluorescence images of sheet-ECM (**a**, **d**, **g**), PCL (**b**, **e**, **h**) and sheet-ECM/PCL (**c**, **f**, **i**) depicting elastic structures induced with a wavelength of 760 nm (green in the overlay) and collagen-containing fibers induced with a wavelength of 840 nm (red in the overlay). Scale bar equals 25 μm.

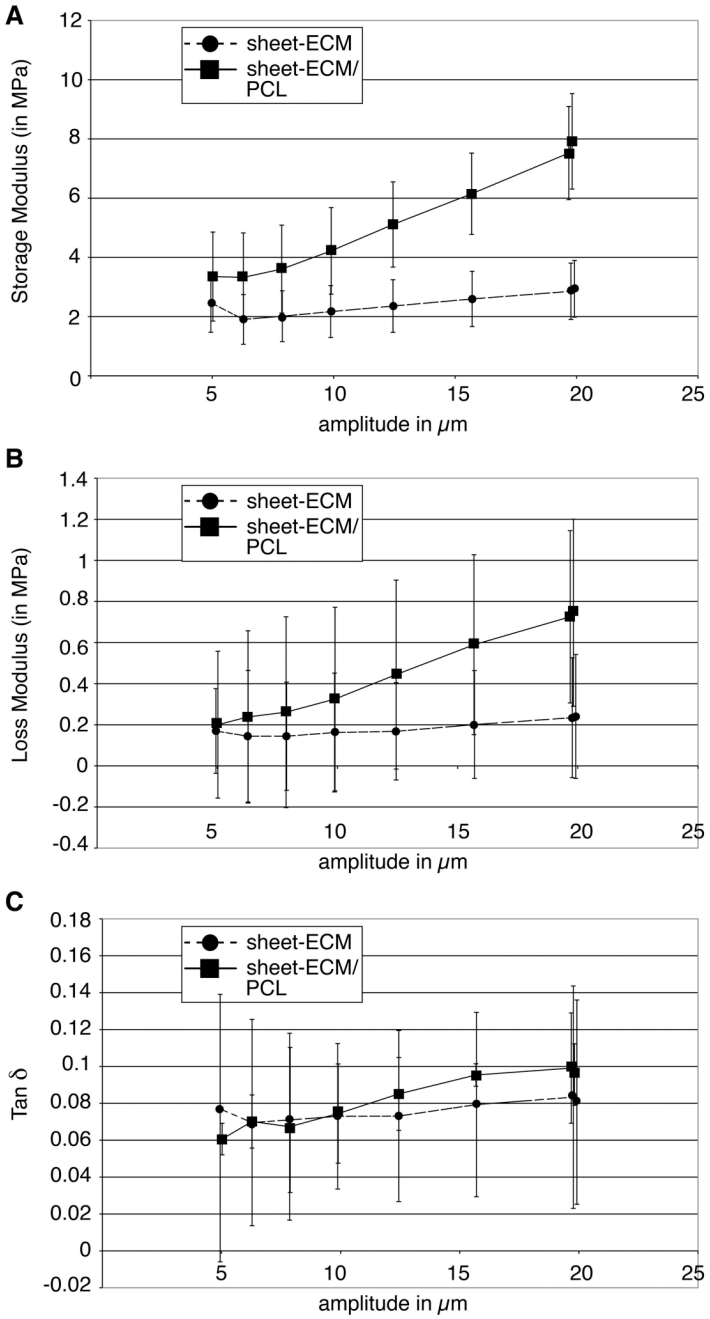

Figure 7.

DMA. (**A**, **B**) The sheet-ECM/PCL hybrid scaffolds demonstrate a significantly higher storage modulus, but also exhibit a significantly higher loss modulus when compared to sheet-ECM alone. (**C**) Tan δ values represent the elastic nature of the scaffolds. Of note, there is a gradual increase in the Tan δ values of both sheet-ECM and sheet-ECM/PCL scaffolds as the strain sweep progresses and the amplitude increase.

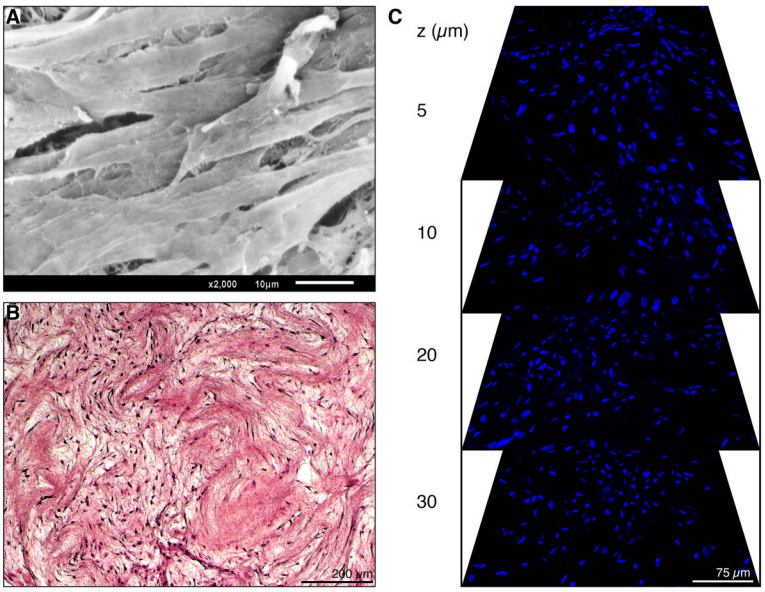

Figure 8.

(**A**) SEM shows cell confluence on the surface of sheet-ECM/PCL scaffolds. Scale bar equals 10 μm. (**B**) H&E-stained section of hASC-seeded sheet-ECM/PCL scaffold that was cultured for 4 weeks. Scale bar equals 200 μm. (**C**) Serial optical horizontal sections taken at depths of 5 μm, 10 μm, 20 μm and 30 μm of the DAPI-stained scaffold show cell migration throughout the entire construct. Scale bar equals 75 μm.

Table 1

Fiber size and pore size. Data are expressed as mean values ± SD.

Scaffold	Fiber size (in μm)	Pore size (in μm^2)
sheet-ECM	0.32 ± 0.05	45.71 ± 0.98
sheet-ECM/ 10%PCL	0.37 ± 0.07	32.24 ± 0.96*

* $P < 0.0001$ compared to sheet-ECM.